Comparison of Two Algorithms for Land Cover Mapping Based on Hyperspectral Imagery

S.S.P. Vithana, A.M.R.Abeysekara, T.S.J. Oorloff, R.A.A. Rupasinghe, H.M.V.R. Herath, G.M.R.I. Godaliyadda, M.P.B. Ekanayake

***Abstract*— This paper presents an analysis of hyperspectral image data, carried out using two approaches followed by a comparison of the two. The hyperspectral image dataset used in this analysis corresponds to a strip along the North Eastern region of Sri Lanka, obtained by the Earth Observing (EO-1) satellite's Hyperion sensor. Mapping land-cover using hyperspectral imagery makes it possible to obtain finer details of land-cover, which are not obtainable using RGB images. Therefore, hyperspectral imagery could be used to obtain useful information for natural resource location and ecosystem service management, assessing the human induced and natural drivers of changes in land, foliage or water bodies and even in the identification of fine details such as the distribution of minerals in an area before doing a ground survey.**

The two algorithms discussed in this paper, initially represent each pixel as a point in a high dimensional space of which the dimensions represent each band of wavelength and subsequently follows two unique approaches to cluster the points (pixels) in a reduced dimensional space. The first algorithm discussed in this paper employs Principal Component Analysis (PCA), Fisher Discriminant Analysis (FDA) and Spectral Clustering in a logical sequence, while the second uses PCA along with concepts of Euclidean geometry. The pixels belonging to each cluster were labeled under 'soil', 'foliage' or 'water bodies', with the aid of the k-means algorithm and the hyperspectral image data of the training set obtained with the aid of Google Maps. The classification process is followed by a comparison of the two approaches employed. Conclusively, the two approaches discussed have their own pros and cons, whilst providing promising results. Hence, both algorithms could be used appropriately based on the application.

Keywords*— *Hyperspectral Imaging, Hyperion, Principal Component Analysis, Spectral Clustering

Manuscript received on 08th Dec, 2017. Recommended by Dr. M. G. N. A. S. Fernando on 12th June, 2018.
This paper is an extended version of the paper "Hyperspectral Imaging Based Land Cover Mapping Using Data Obtained by the Hyperion Sensor" presented at the ICTer 2017.

S.S.P. Vithana, A.M.R.Abeysekara, T.S.J. Oorloff and R.A.A. Rupasinghe hold B.Sc. Special Degrees in Electrical and Electronic Engineering from University of Peradeniya. (*saj3jas@gmail.com, ruwanthiabeysekara@gmail.com, shaneoorloff@gmail.com, ra.anuththara@gmail.com*).
H.M.V.R. Herath, G.M.R.I. Godaliyadda and M.P.B. Ekanayake are Senior Lecturers at the Department of Electrical and Electronic Engineering of University of Peradeniya. (*vijitha@eng.pdn.ac.lk, roshangodd@ee.pdn.ac.lk, mpb.ekanayake@ee.pdn.ac.lk*).

I. Introduction

A hyperspectral image is a collection of high resolution monochromatic pictures depicting the reflectance values corresponding to a broad range of wavelengths. Hyperspectral images measure reflected radiation at a series of narrow and contiguous wavelength bands. This enables the selection of appropriate frequency bands, which carry the characteristic information of a given pixel. Multispectral images differ from hyperspectral images as, even though the images are obtained in more than one spectral band, they are non-contiguous in their coverage of the spectrum.

There are three main methods of representing hyperspectral data. The first is, by the use of a hypercube, of which the XY plane corresponds to the pixel coordinate plane and the Z axis corresponds to the wavelength (in a conventional XYZ three dimensional space). It is formed by stacking the images obtained at contiguous spectral bands in sequence. Hyperspectral image (HSI) data can also be represented as a spectral signature, which is a reflectance spectrum, where the reflectance values are plotted against the wavelengths. The third method is, representing pixels as points on a higher dimensional Euclidean space where the axes corresponds to the reflectance values of each spectral band.

The reflectance values in hyperspectral images mainly depend on the type of material (chemical composition) and its physical structure. The reflectance spectrum of a pixel is formed as a result of superposition of many reflectance spectra of the sub-pixel materials known as end-members in the area covered by the pixel. Further, the reflectance value mainly depends on the type of material (chemical composition) and its physical structure. As hyperspectral imagery enables analysis of images obtained at a large number of narrow contiguous spectral bands, many fine, accurate and precise information could be obtained through HIS, which would not be possible through multispectral imaging as RGB imaging. Further, hyperspectral image analysis enables detection of features using remote sensing, which is a non-intrusive method as other image analysis techniques but with a high degree of accuracy and a higher degree of detail. The popular applications of HSI include, feature detection of human faces (facial recognition), object identification, food quality detection, biomedical applications, mineral identification and land cover mapping.

Land cover mapping using hyperspectral image data has its own merits and demerits. Since the finest details of the images are available, the accuracy of the classification is high when the ideal spectral bands are chosen. It is also possible to extract information about the images that are not conveyed through RGB images. However, the redundancy of data, complexity in computations and excessive memory usage are among the disadvantages of using Hyperspectral Imaging (HSI) data for land cover mapping [1]–[3].

In this paper, the HSI data which was obtained by the Earth Observing - 1 (EO - 1) satellite's Hyperion sensor [4] has been used to classify the pixels under soil, water and foliage in two different algorithms. The first algorithm consists of two stages. The first stage is used to classify pixels containing water and the next stage classifies the pixels containing soil and foliage, which are not easily separable. This algorithm requires a greater degree of computational power due to its advance

mathematical operations. The second algorithm however, is more simple and is mainly based on Euclidean geometry. The sensor that was used in imaging is capable of resolving more than 200 spectral bands (from 0.4 to 2.5 µm) with a 30-meter resolution. The instrument has the ability of imaging a 7.5 km by 100 km land area per image, while providing a detailed spectral mapping across all channels with high radiometric accuracy. The telescope provides for two separate grating image spectrometers to improve signal-to-noise ratio (SNR). Low SNR sub-bands within the HSI band have no effect on the final result of classification. Hence, they were eliminated in the pre-processing stage.

The previous work carried out on the topic is described in section II. The study area and the dataset are presented in the section III. The technique used to preprocess data is discussed in the section IV. Algorithms used in this work are discussed in the section V under methodology. Results are presented and discussed in the sections VI and VII. Concluding remarks are made in the section VIII.

II. Related Work

According to the previous work done on land cover mapping based on Hyperspectral imaging, comparisons have been made on the performance of a hierarchical algorithm which is used for land cover mapping, with the aid of hyperspectral and multispectral data of the same image [5]. The algorithm has used classical dimensionality reduction techniques such as Principal Component Analysis (PCA), Linear Discriminant Analysis (LDA) and Penalized Discriminant Analysis (PDA), followed by Mahalanobis Distance (MD) classifier, to perform the land cover classification.

An algorithm for land cover mapping using HSI data based on neural networks has been proposed previously[5],[6], in which the neural network is trained by a set of samples taken from the image itself. The inherent tendency of parallel implementation in hyperspectral images, has been exploited in this algorithm.

Many algorithms on feature detection based on HSI, have been developed in the recent past using modern optimization techniques. An algorithm for sub pixel mapping based on particle swarm optimization, named Modified Binary Quantum Particle Swarm Optimization (MBQPSO) has been proposed in 2017 [7]. Its main focus is on the discretization of Quantum Particle Swarm Optimization (QPSO) which is implemented by modifying the discrete update process of particle location, to minimize the objective function, which is formulated based on different connected regional perimeter calculating methods.

HSI analysis based through machine learning classifiers has been presented in the literature, where Support Vector Machines (SVM) and Artificial Neural Networks (ANN) are used [8]. It compares the accuracy of the two methods while presenting a universal feature detection technique. It has also concluded that SVM outperforms ANN in land cover classification, due to the ability of the SVM classifier to identify an optimal separating hyperplane for class separation, which allows a low generalization error, thus producing the best possible class separation. It further identifies a drawback in both SVM and ANN. That is, the inability of both the classifiers to operate on a sub-pixel level, which can significantly reduce their accuracy due to possible mixture problems that occur when coarse spatial resolution remote sensing imagery is used.

In this paper, we propose two algorithms in order to detect features in hyperspectral images. The first algorithm is unique to the dataset under consideration, which results in a highly precise classification. The second is a more generalized and a simple algorithm which requires less amount of computational power. The two algorithms are compared and contrasted, while logically reasoning out each step in them. These algorithms and the concepts behind them can be adjusted to fit any HSI dataset of interest based on the affinity of the data points represented in a high dimensional space.

III. Study Area and Data Set

The area of interest of our study comprises of a strip along the North Eastern region of Sri Lanka as depicted in the figure 1.

The Hyperion image of the aforementioned region shown in figure 1 (a) and of geographical coordinates as in Table I, had been acquired on the 17th of September, 2005 starting at 04:40:57 and ending at 04:45:35 in local time (+5:30 GMT). Two cameras, VNIR (Visible and Near-Infrared) and SWIR (Short Wave Infrared) had been used to obtain the hyperspectral images of 242 bands spanning across a range of wavelengths, from 355.59nm to 2577.08nm [8]. However, 44 spectral bands have not been calibrated and cannot be used for data analysis. Low SNR sub-bands which provides inaccurate radiance values are eliminated in the pre-processing stage, in order to avoid inaccuracies in the classification process.

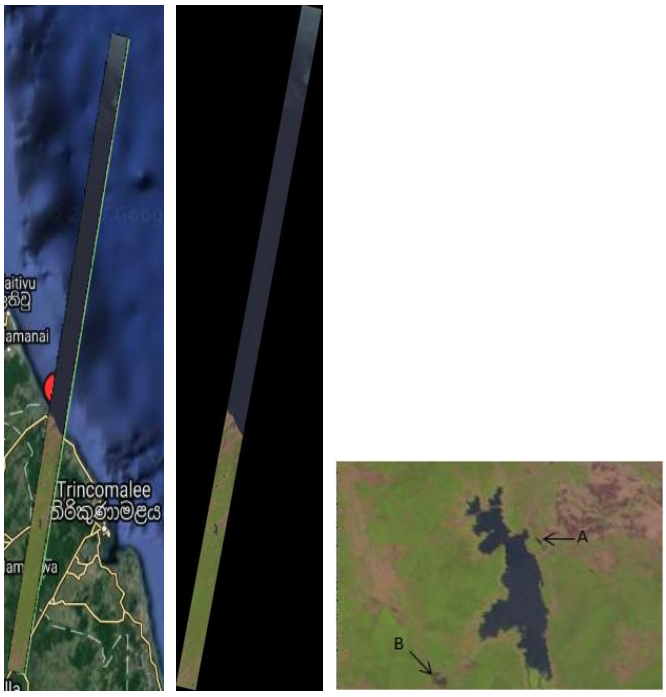

(a) (b) (c)

Fig. 1 (a) The geographical location of the study area (b) True color satellite image (c) The area chosen for classification

TABLE I
LATITUDES AND LONGITUDES OF THE SELECTED REGION

	Latitude/°N	Longitude/°E
Upper left corner	10.146810	81.251940
Upper right corner	10.133729	81.319533
Lower left corner	8.137243	80.818856
Lower right corner	8.124515	80.886088

TABLE II
THE STRUCTURE OF DATA FILES

Col no.	**Availability of Neighbouring pixel information**								**Spectral information**			
	N	**NE**	**E**	**SE**	**S**	**SW**	**W**	**NW**	**1**	**2**	**-**	**242**
1st index	-	-	-	-	-	-	-	-	-	-	-	-
2nd index	-	-	-	-	-	-	-	-	-	-	-	-
3rd index	-	-	-	-	-	-	-	-	-	-	-	-
-	-	-	-	-	-	-	-	-	-	-	-	-
262nd index	-	-	-	-	-	-	-	-	-	-	-	-

The Geo 'TIFF' images representing intensities of each spectral band, contained 7481 X 1851 pixels of which each pixel covers a geographical area of 30m X 30m. The data included in the images were radiance values of the respective wavelengths scaled by 40 for images obtained through the VNIR camera in the range of wavelengths from 400 nm to 1400 nm (bands 1 - 70) and by 80 for images obtained by the SWIR camera in the range of wavelengths from 900 nm to 1700 nm (bands 71 - 242).

IV. PRE-PROCESSING

Pre-processing is deemed to be an important stage prior to any data analysis with the intention of providing qualitative and more productive data [9]. Pre-processing included extraction of data in a useful manner while removing the uncalibrated sets of data as indicated in [4] and conversion of the radiance values of the Geo 'TIFF' images to reflectance.

A. Extraction of Data

As seen in figure 1 (b), it is well evident that the useful information in the image is limited to a much less region compared to the total size of the image (approximately 14%). Hence, in order to improve efficiency and to use the memory optimally, the important data were extracted in the following manner.

MATLAB® variable files (.mat) containing arrays of size 262 x 251 each, were created for each information containing row of the image in the structure shown in Table II (as there are 262 pixels per row and 251 spectral bands containing reflectance information).

Finally, the uncalibrated data were removed creating a final matrix of size 262 X 207.

B. Radiance to Reflectance Conversion

In Hyperspectral image analysis reflectance values of closely lying bands are used and hence the radiance values obtained from the raw data set had to be converted into reflectance prior to any process of analyzing. The conversion process was done using,

$$\rho = (\pi . L_\lambda . d^2) / (ESUN_\lambda . cos\, \theta_s), \quad (1)$$

where,

ρ: unitless planetary reflectance,
L_λ: spectral radiance at the sensor's aperture,
d : Earth-Sun distance in astronomical units,
$ESUN_\lambda$: Mean solar exoatmospheric irradiances,
θ_s: Solar zenith angle in degrees.

By substituting the spectral radiances obtained from the extracted data upon scaling with the scaling factors provided for the respective range of wavelengths, (1/40 for the first 70 spectral components and 1/80 for the rest) the earth-to-sun distance [10], mean solar exo-atmospheric irradiances [10] and the Solar zenith angle based on the location, date and time of which the images were captured [11], the respective reflectance values were obtained. Since the image spans across a small region and as the zenith angle does not vary considerably in the range of interest, the zenith angle was assumed to be constant throughout the region of interest.

Figure 2 shows the spectral signatures of the three classes, soil, foliage and water considering reflectance values calculated for 198 spectral bands (this was obtained by considering 20 training samples from each class). As 30 of the spectral bands had SNR values under 30, associated with their radiance measurements in the sensor, the reflectance information obtained for these 30 bands were removed at this stage, since the accuracies of such low SNR bands cannot be guaranteed. The SNR distribution of the Hyperion sensor, among the spectral bands is shown in figure 3 [12], and the resulting spectral signatures with the low SNR bands removed is illustrated in figure 4.

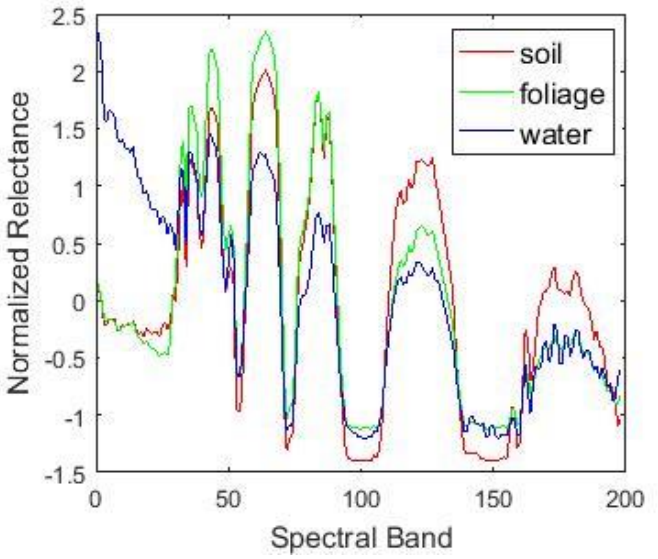

Fig 2: Spectral signatures of the three classes, soil, foliage and water

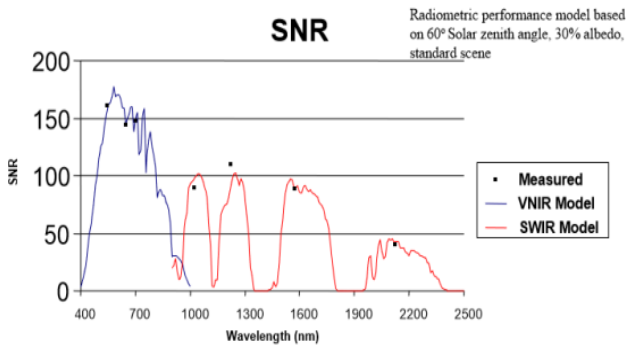

Hyperion Measured SNR						
550 nm	650 nm	700 nm	1025 nm	1225 nm	1575 nm	2125 nm
161	144	147	90	110	89	40

Fig 3: Signal to noise ratio of each spectral band in the Hyperion sensor

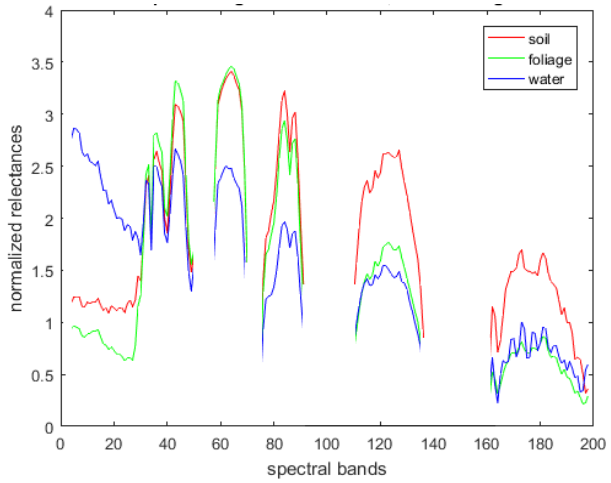

Fig 4: Spectral signatures of the three classes, soil, foliage and water with the low SNR components removed

V. Methodology

The part of the image under consideration, shown in figure 1 (c), contained a total of 175 x 251 (i.e. 43925) pixels. Each pixel was classified under 'soil', 'foliage' or 'water bodies', based on their hyperspectral image data, using the tools available in MATLAB®. As discussed in the pre-processing section, the HSI data of each row of pixels in the image is tabulated in a separate table in the form of '.mat' files. Each table was then loaded to MATLAB® and was stored in the form of a two dimensional matrix, representing its pixels and their spectral data in its two dimensions.

The task of classifying each pixel in the image under soil, foliage or water, was performed using two different approaches. The first approach is a two-stage process where pixels containing water, are identified first and the rest of the classification is performed in the second stage. The second approach is a direct classification of pixels in the image under the three classes, soil, foliage and water, based on a measure of disparity.

A. Approach 1:

First, in order to understand the nature of the dataset and to come up with spectral signatures for each of the classes, soil, foliage and water, a training sample of pixels were obtained from the image with the aid of google maps and the image processing toolbox available in MATLAB®. Sixty pixels were chosen from the image, containing 20 pixels from each of the classes, soil, foliage and water bodies [13]. The spectral information of the training set was normalized with respect to the standard deviation of each pixel's reflectance values to ensure the dataset used for analysis is unbiased. Mean spectral signatures which are depicted in figure 4 for each class was then obtained by calculating the mean of the 20 pixels belonging to each class, in the training set.

The spectral signatures of the three substances show that soil and foliage have similar spectral characteristics while water is slightly deviated from the other two. Due to this factor, it was decided that the classification should be done in a series of two stages,

Stage 1: determining the pixels containing water

Stage 2: determining the pixels containing soil and foliage

1) Stage 1:

Each pixel of this image contains spectral information of 168 frequency bands, after the elimination of the low SNR bands. The spectral information of each pixel was represented as a point in the Euclidean space with the frequency bands as its dimensions. Data processing in the 168 dimensional original space is ineffective in terms of computational power as well as feature detection, as it contains both relevant and irrelevant information. Hence, the feature space needs to be transformed to a lower dimensional space that maximizes the separation between pixels in general, while maximizing the between class separation and minimizing the within class separation. In order to find the transformation matrix for dimensionality reduction, Principal Component Analysis (PCA) [3], [14], [15] and Fisher Discriminant Analysis (FDA) [16]–[18] were performed on the training dataset. The final transformation matrix which is used for dimensionality reduction contains two transformation matrices. PCA generates the first transformation matrix that transforms the original feature space to a space where the pixel scatter is maximized [15].

The PCA equations are as given by,

$$C = E\{(X_n - \mu)(X_n - \mu)^T\} \quad (2)$$

$$C = \frac{1}{N}\sum_{n=1}^{N}(X_n - \mu)(X_n - \mu)^T \quad (3)$$

$$CM = \lambda M \quad (4)$$

where,

C : covariance matrix, (168×168),
E : expected value operation,
X_n: vector representing the normalized 168 spectral band information (reflectance) of a pixel, (168×1),
μ : vector representing the mean spectral information (normalized reflectance) of all pixels, (168×1),
N : number of pixels in the training sample (60),
M : eigenvector of the covariance matrix, (168×1),
λ : eigenvalue of the covariance matrix.

The eigenvectors corresponding to equation (3) give the principal components of a given system. In dimensionality reduction using PCA, the directions that have a maximum variation of data points, are chosen to create the new Euclidean space with reduced number of dimensions. Here the first 20

principal components (eigenvectors), corresponding to the largest 20 eigenvalues were selected. The objective of finding the set of directions that maximizes the scatter of data points in Euclidean space with a significant improvement, compared to the other directions, which were there in the original space, is met by this approach, as the eigenvalue is a measure of the variation of data points, in the direction of its respective eigenvector. Using this method, the first transformation matrix of size 20 x 168 was created. This reduces the feature space dimensions from 168 to 20 using the transformation matrix,

$$\Gamma_1 = [M_1\ M_2\ M_3 \dots M_{20}]^T \quad (5)$$

where,

Γ_1: Transformation matrix based on PCA,
$M_1, M_2, M_3 \dots M_{20}$: eigenvectors of the covariance matrix.

In the original space, the spectral information of a pixel was represented by a vector of size (168×1). Using the above transformation, each pixel was transformed into the new space of 20 dimensions using

$$V_1 = [M_1\ M_2\ M_3 \dots M_{20}]^T V \quad (6)$$

where,

V : Matrix representing the pixels (in columns) in the original space,
V_1: Matrix representation of pixels (in columns) in the reduced space.

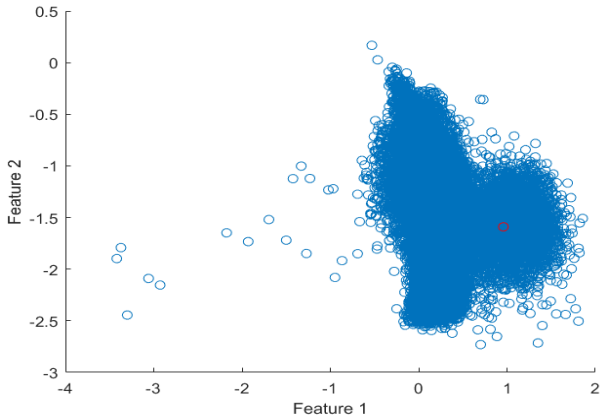

Fig 5: Scatter of all the pixels in the image in the reduced space. *The point in red represents the mean spectral signature of water in the reduced space*

Fig 6: Classification of pixels containing water. *Pixels that contain water are shown in white while other pixels are shown in black*

The second transformation matrix was obtained using FDA. FDA maximizes between-class scatter of pixels while minimizing the within-class scatter of pixels. FDA equations are as given by,

$$S_b = \sum_{i=1}^{l} n_i(\mu_i - \mu)(\mu_i - \mu)^T \quad (7)$$

$$S_w = \sum_{i=1}^{l} \sum_{j \in i} (x_j - \mu_i)(x_j - \mu_i)^T \quad (8)$$

$$\mu_i = (1/n_i) \sum_{j \in i} x_j \quad (9)$$

$$\mu = (1/n) \sum_{i=1}^{n} x_i \quad (10)$$

$$S_b \varphi = \lambda S_w \quad (11)$$

where,

S_b : between class scatter matrix (20×20),
μ : vector representing mean spectral information of all pixels (20×1),
μ_i : vector representing mean spectral information of the pixels of class i (20×1),
n_i : number of pixels in the training sample belonging to class i (20),
l : number of classes (3),
S_w: within class scatter matrix (20×20),
x_j : vector representing the spectral information of a pixel In the training sample belonging to class i (20×1),
λ: eigenvalues of the fisher matrix, $S_w^{-1}S_b$,
φ : eigenvectors of the fisher matrix, $S_w^{-1}S_b$.

The Fisher matrix, $S_w^{-1}S_b$ of the training dataset was of rank two, which resulted in only two real eigenvalues of the Fisher matrix. This further implies the similarity between the spectral characteristics of pixels containing soil and foliage, resulting in a combined class. Hence, the second transformation matrix,

$$\Gamma_2 = [\varphi_1\ \varphi_2]^T \quad (12)$$

where,

Γ_2 : Second transformation matrix,
φ_1, φ_2: real eigenvectors of the Fisher matrix,

was obtained using the first two eigenvectors of the Fisher matrix, corresponding to the two real eigenvalues.

The vectors that represent the pixels in the 20 dimensional space is now reduced to a two dimensional space, using the second transformation. The transformed pixels in the new space are given by,

$$V_2 = [\varphi_1\ \varphi_2]^T V_1 \quad (13)$$

where,

V_1 : matrix representing the pixels in the 20 dimensional space ,
V_2 : matrix representing the pixels in the 2 dimensional space, after PCA and FDA.

The scatter plot representing all the pixels in the image is shown in figure 5.

By observing the scatter plot, the pixels belonging to the classes ‘water’ and ‘not water (i.e. soil and foliage)’ can be identified as two clusters. Using a threshold of 0.485 (based on

observations of the scatter plot) as the radius, pixels within a circle with its center as the point representing the spectral signature of water in the reduced space and the radius mentioned previously, were identified as the pixels that contain water in them. The figure 6 shows the results of stage 1, the classification of pixels under 'water' and 'not water'

2) Stage 2:

In this stage, the pixels that do not contain water in them were extracted which summed up to a total of 39968 pixels, for further classification under soil and foliage. Since the spectral signatures of soil and foliage were very much similar to each other, a different approach needed to be taken. Spectral bands ranging from the 100th to the 168th were chosen for the classification process, as in that range, a significant variation of spectral characteristics of soil and foliage could be observed (figure 4). No further dimensionality reduction was used in this stage. Instead, to capture the slight variations of the spectral characteristics, spectral clustering was used [19]–[21]. In this, the points in the 69 dimensional space, representing each pixel of the image (except the pixels containing water) were clustered into two groups, based on their similarity in Hyperspectral Image characteristics. The first step of this method was to generate the disparity matrix. Due to the limitations of processing power and the size of matrices that MATLAB® could handle, the total of 43925 pixels were divided into 6 sets of 5700 pixels, and the 7th set containing 5768 pixels. The disparity matrix contains the Euclidean distance between each pixel pair, corresponding to the row number and the column number in each entry of the matrix. i.e. The (42,19)th element on the disparity matrix indicates the Euclidean distance between the points that represent the 42nd and the 19th pixels. Smaller the value in the cell, greater the similarity between the two pixels. Figure 7 shows the disparity matrix corresponding to the first set (pixels of the first 25 rows).

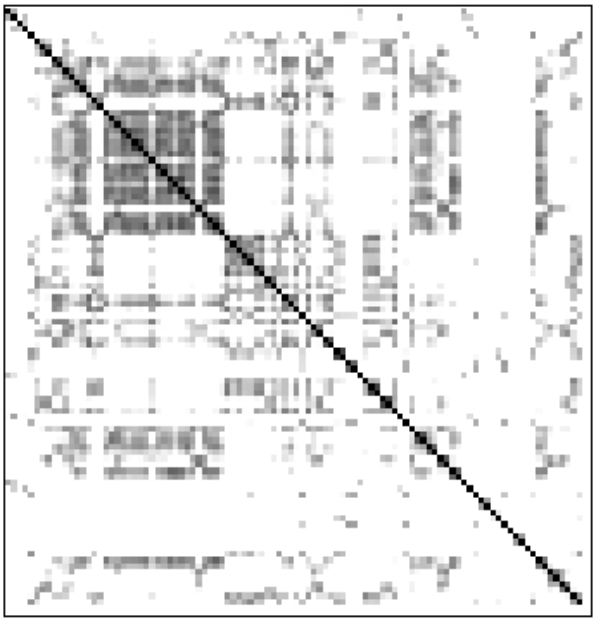

Fig 7: Disparity matrix of the pixels in the first 25 rows of the considered region in the image. *The darker regions indicate smaller values of distances while the lighter regions indicate otherwise*

The entries in this matrix were normalized by the largest value in the matrix, for better accuracy. The Gaussian kernel [19]–[21] was then applied to the values in the matrix, to generate the affinity matrix, which indicates the closeness of pixels i and j, by its (i,j)th element.

The Gaussian kernel is given by,

$$a(i,j) = e^{-\frac{d(i,j)^2}{2\sigma^2}} \quad (14)$$

where,

a(i,j) : (i,j)th entry in the affinity matrix,
d(i,j) : (i,j)th entry in the disparity matrix.

The value of σ was obtained as follows. As the objective was to classify each pixel under soil and foliage, the resulting number of clusters obtained from spectral clustering should be two. Further, the affinity matrix should have two significant eigenvalues. This could be understood by an ideal situation where the affinity matrix would be as the one shown below.

$$\begin{bmatrix} 1 & 1 & 1 & 1 & 0 & 0 & 0 & 0 & 0 \\ 1 & 1 & 1 & 1 & 0 & 0 & 0 & 0 & 0 \\ 1 & 1 & 1 & 1 & 0 & 0 & 0 & 0 & 0 \\ 1 & 1 & 1 & 1 & 0 & 0 & 0 & 0 & 0 \\ 0 & 0 & 0 & 0 & 1 & 1 & 1 & 1 & 1 \\ 0 & 0 & 0 & 0 & 1 & 1 & 1 & 1 & 1 \\ 0 & 0 & 0 & 0 & 1 & 1 & 1 & 1 & 1 \\ 0 & 0 & 0 & 0 & 1 & 1 & 1 & 1 & 1 \\ 0 & 0 & 0 & 0 & 1 & 1 & 1 & 1 & 1 \end{bmatrix}$$

It is clear that pixels 1,2,3 and 4 belong to the same class and the rest of the pixels belong to another class, according to the above affinity matrix. Moreover, the eigenvalues of the above matrix are 4,5,0,0,0 and 0. This ideal situation shows that the number of clusters equal the number of significant eigenvalues of a given affinity matrix. Using this observation, in order to find out the optimum value of σ, that would cluster the sets of pixels in Euclidean space into two significant clusters, (soil and foliage) the eigenvalues of the affinity matrix, for a range of σ values were obtained. The second eigen gap (difference between the second and the third largest eigenvalues) of the affinity matrix for each σ value was plotted to find out the optimum value for σ, that would result in the two most significant clusters. Since the number of significant eigenvalues of the affinity matrix describes the number of clusters, the σ value at which the second eigen gap of the affinity matrix maximizes, is the value of σ that gives the two most significant eigenvalues in the corresponding affinity matrix, resulting in two significant clusters of pixels. Figure 8 shows the sigma selection process

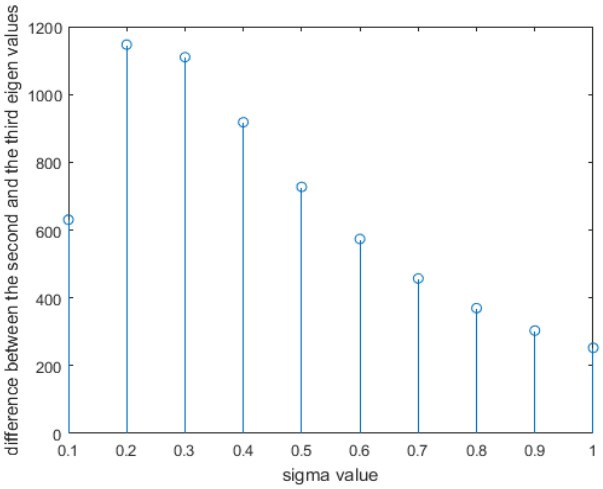

Fig 8: Variation of the second eigen gaps of the affinity matrix, for a range of σ values. *In this case the highest 2nd and 3rd eigenvalue gap is obtained at* σ=0.2 *Hence this value is selected for* σ *in the next steps of spectral clustering*

After selecting the optimum σ, the affinity matrix was obtained using equation (14). The eigenvectors of the affinity matrix found using,

$$AV = \alpha V \tag{15}$$

where,

A : affinity matrix of the first 5700 set of pixels,

V: eigenvectors of A,

α : eigenvalues of A.

corresponding to the two most significant eigenvalues were stacked as columns in the matrix X as,

$$X = [\, v_1 \; v_2 \,] \tag{16}$$

where,

X : transformation matrix that maps the pixels to a new space ,

N : number of pixels in a block,

v_1, v_2 : the eigenvectors corresponding to the two largest eigenvalues of A.

which represents each pixel by its rows. Since spectral clustering was performed separately on blocks of pixels of the image, this would only give the representation of 5700 pixels in the new two dimensional space at once.

Each row of matrix, X would be the new representation of each pixel in the new two dimensional space. In this reduced space, the points representing the pixels would be clustered into two groups, based on its hyper spectral characteristics.

Using K-means algorithm [22], the two clusters were identified. The vector that represents the spectral characteristics of the mean of the pixels belonging to a cluster identified above, in the original space, was then calculated. Depending on the Euclidean distance between the mean vector of the cluster and the vectors representing the spectral signatures of soil and foliage in the original space, each cluster was identified as 'soil' or 'foliage' such that the error in terms of Euclidean distance between the cluster mean and the means of foliage and foliage. The same classification process was repeated for the seven blocks. Finally, each pixel of the image which was classified under water, soil or foliage was assigned a number based on its content, to recreate the image, based on the results obtained by the analysis of hyperspectral information of each pixel.

B. *Approach 2:*

Reflectance values of 168 spectral bands, for each pixel in the image, were available after the pre-processing stage. These reflectance values of each pixel, were arranged in an array, to generate its spectral signature. In order for the classification to be solely dependent on the spectral characteristics of the image, these spectral signatures were normalized, by removing its mean and by scaling it using its standard deviation. The resulting normalized reflectance values of each pixel was represented as a point in a 168 dimensional space, where the dimensions corresponded to the reflectance values of each of the spectral bands.

In order to detect fine features of the image, and due to the redundancy of information, the data set was transformed into a 20 dimensional space, using Principal Component Analysis. (PCA) [3], [14], [15] . To find the transformation matrix for the dimensionality reduction, a training sample of 60 pixels were chosen, 20 from each class [13], as discussed in approach 1. The spectral signatures of the three classes based on the training sample data (considering the original spectral space) are shown in figure 2. The reduced space was obtained by using the PCA equations [3], [14], [15] discussed in approach 1.

All the pixels including the training sample, were transformed to the new reduced dimensional space using equation 6. The pixels are now represented as points (vectors directing to specific points) in a 20 dimensional space. The direction of each of these vectors mainly characterizes the spectral behaviour of the pixels. The magnitude of these vectors however carries spectral information as well as other effects of the sensing equipment, environmental conditions etc. Based on that conclusion, the direction of the vectors was considered as the basis of the classification algorithm. Thus, the vectors representing all the pixels, including the training sample, were divided by its magnitude to convert them into unit vectors. Now all the pixels are represented as points (unit vectors directing to each of the points) on the surface of a sphere of unit radius, in a 20 dimensional space. The equation for obtaining the unit vectors is given by,

$$\boldsymbol{\omega} = \frac{\boldsymbol{w}}{|\boldsymbol{w}|} \tag{17}$$

where,

$\boldsymbol{\omega}$: Unit vector in the reduced space

$\boldsymbol{w}$: Original vector in the reduced space

$|\boldsymbol{w}|$: Magnitude of the original vector in the reduced space

For each of the three classes, soil, foliage and water, three reference unit vectors, representing the spectral signatures of the three classes, were generated. This was done by calculating the mean of the 20 unit vectors corresponding to the 20 training samples selected from each class. The difference between each vector representing a pixel on the unit sphere and the three reference vectors were calculated to form a distance vector for each pixel, which is given by

$$\boldsymbol{\delta} = (|\boldsymbol{\omega} - \boldsymbol{\omega_s}| \ |\boldsymbol{\omega} - \boldsymbol{\omega_v}| \ |\boldsymbol{\omega} - \boldsymbol{\omega_w}|)^T \quad (18)$$

where,

$\boldsymbol{\delta}$: the distance vector
$\boldsymbol{\omega}$: unit vector representing a given pixel
$\boldsymbol{\omega_s}$: unit vector representing the reference spectral signature of soil
$\boldsymbol{\omega_v}$: unit vector representing the reference spectral signature of vegetation
$\boldsymbol{\omega_w}$: unit vector representing the reference spectral signature of water.

Since the requirement is to obtain a measure of affinity, the reciprocals of the distances were considered for the classification. The vector representing the percentage affinity of a given pixel, to the reference spectral characteristics of the three classes is given by,

$$\boldsymbol{\gamma} = \begin{matrix} \frac{\frac{1}{|\omega-\omega_s|}}{\frac{1}{|\omega-\omega_s|}+\frac{1}{|\omega-\omega_v|}+\frac{1}{|\omega-\omega_w|}} \\ \frac{\frac{1}{|\omega-\omega_v|}}{\frac{1}{|\omega-\omega_s|}+\frac{1}{|\omega-\omega_v|}+\frac{1}{|\omega-\omega_w|}} \\ \frac{\frac{1}{|\omega-\omega_w|}}{\frac{1}{|\omega-\omega_s|}+\frac{1}{|\omega-\omega_v|}+\frac{1}{|\omega-\omega_w|}} \end{matrix} \quad (19)$$

where,

$\boldsymbol{\gamma}$: percentage affinity vector and the other terms are the same as before.

The class of each pixel was determined by the index corresponding to the maximum component of the affinity vector.

$$I = \arg(max(\boldsymbol{\gamma})) \quad (20)$$

where τ is the index corresponding to the maximum affinity percentage of the affinity vector.
The pixels were labelled according to the following criteria where,

if $I = 1$ the pixel under consideration is classified under soil,
if $I = 2$ the pixel under consideration is classified under foliage, and
if $I = 3$ the pixel under consideration is classified under water.

VI. Results

A part of the image of a strip along the North Eastern region of Sri Lanka, taken by the Earth Observing - 1 satellite's Hyperion sensor was classified under soil, water and foliage, based on the HSI data of the image. The portion of the image that was considered in the classification consisted of 43925 pixels in total. The classification was performed in two different approaches. The first is a two-stage algorithm, which is based on classical feature reduction techniques employed in a logical sequence. The results of this approach are tabulated in Table III and represented using a pie chart as in figure 9. The second approach is a single stage approach which is developed upon a disparity measure. The results of the second approach are shown in table IV and figure 10. The two recreated images of the area, using approach 1 and 2 are shown in figures 11 and 12 respectively, in which soil is represented in black, foliage in grey and water in white. These recreated images are comparable with the original true color RGB image in figure 1 (c).

TABLE III
Number of Pixels belonging to each Class using approach 1

Substance	***Soil***	***Foliage***	***Water***
Number of pixels	15651	24317	3957

TABLE IV
Number of Pixels belonging to each Class using approach 2

Substance	***Soil***	***Foliage***	***Water***
Number of pixels	13236	27026	3663

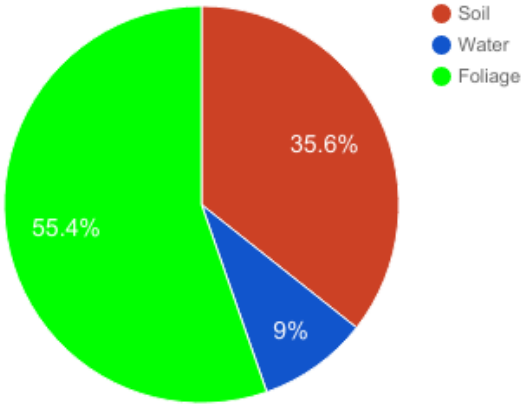

Fig 9: Percentage of each substance in the chosen part of the image using approach 1

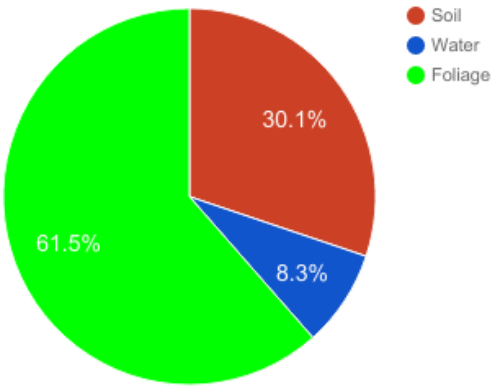

Fig 10: Percentage of each substance in the chosen part of the image using approach 2

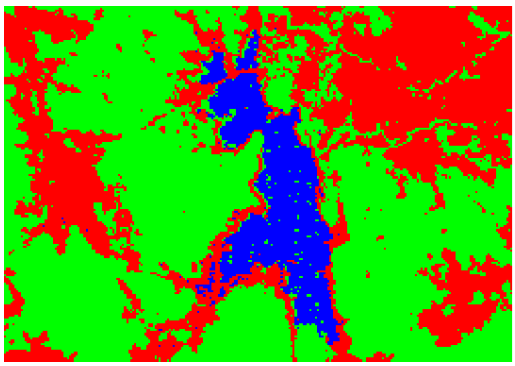

Fig 11: Recreated image based on the results of classification using approach 1

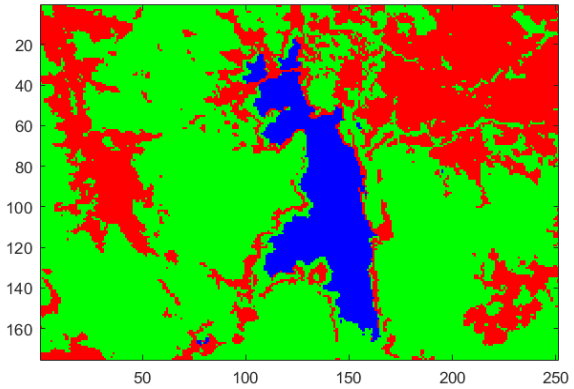

Fig 12: Recreated image based on the results of approach 2

VII Discussion

Overall, the two approaches give similar results. However, approach 1 seems to be capturing minute details of the image, as opposed to approach 2. This is evident from the two recreated images, as the image recreated from approach 1 contains more fine details, compared to that of approach 2. More specifically, the foliage contents inside the main water body in the middle, which are captured by approach 1, are absent in the image recreated using approach 2. This can be explained by the nature of the two algorithms. The first approach is custom made for this dataset as it takes the nature of the spectral signatures of the three substances present in the dataset in to account, and breaks down the classification process into a number of stages accordingly. After the first stage in which the pixels belonging to a class, which is easily separated are identified, the pixels which can be mixed in its representation in the higher dimensional space are analyzed more specifically in the second stage. Classical clustering algorithms with logical methods of determining its parameters, are used in the second stage of the first approach. Hence, the advanced analysis and techniques used in approach 1, have resulted in the fine details that can be observed in figure11. On the other hand, approach 2 uses a simple affinity based measure, developed upon the Euclidean distance between the vector representation of each pixel and the reference vectors of the three classes, to classify each of the pixels under soil, foliage or water. This requires a relatively small amount of computational power, and can be used on any data set of interest.

As the data set does not provide ground truth information, a standard accuracy level cannot be calculated in this work. However, a visual validation of results can be carried out by comparing the two resulting recreated maps with the real image shown in figure 1(c). Also, it could be noted that the subtle details of the image such as the small water bodies marked as A and B in figure 1(c) have also been identified in the proposed technique, which is evident in figures 11 and 12.

As the size of a pixel is 30m x 30m, it is highly likely that a single pixel could contain more than one substance. In this case, the affinity vector introduced in approach 2 can be used to calculate the approximate percentage of each substance (soil, foliage and water) in a given pixel which contains a mixture of two or more substances [23].

VIII Conclusion

Using hyperspectral imagery in order to map land-cover maps is beneficial in many ways as it could be used as a basis to obtain useful information for natural resource and ecosystem service management, assessing the human induced and natural drivers of changes in land, foliage or water bodies and even in identification of fine details such as the distribution of minerals in an area. Use of hyperspectral image data in land cover mapping results in better classification as it contains fine data which is necessary for fine classification. The image considered in this paper consisted of 198 spectral bands which had calibrated data. Hence, it was possible to select the most useful spectral bands for a better classification. However, the excess information could also be challenging, especially in cases with computational limitations. In this paper, two algorithms were presented to classify each pixel of the image under soil, foliage or water. The first algorithm was based on classical dimensionality reduction and classification techniques such as PCA, FDA, spectral clustering and K-means that have been used in a logical manner as explained in the body of the paper. Based on this algorithm, the pixels of the image were classified in two steps. First the pixels containing water were identified. Thereafter, pixels containing soil and foliage were classified. This two-stage approach was taken due to the nature of the hyperspectral data of the pixels which was observed by the spectral signatures obtained by the training samples and was justified based on the rank of the Fisher matrix. The second classification algorithm was based on a measurement of affinity between the vector representations of each pixel and the three reference vectors corresponding to soil, foliage and water. Both the approaches resulted in recreated images similar to the true RGB image. However, the first approach was capable of identifying the fine details of a given hyperspectral image whereas the second approach failed to achieve that. On the other hand, the first algorithm was custom made for this data set and required high computational power due to its higher complexity. The second algorithm however could be used on any hyperspectral image dataset with less amount of computational power. Hence, it could be concluded that, according to their merits and demerits, the algorithm or the concepts behind the algorithms that suit the best for a given classification task may vary depending on the application and the constraints associated with it.

ACKNOWLEDGEMENT

We are immensely grateful to the United States Geological Survey (USGS) for making available the Hyperspectral images obtained by the EO - 1 satellite's Hyperion sensor and other related data which were used in applying the algorithm discussed in this paper.

REFERENCES

[1] M. Clark and N. Kilham, "Mapping of land cover in Northern California with simulated hyperspectral satellite imagery," *ISPRS J. Photogramm. Remote Sens.*, vol. 119, pp. 228–245, 2016.

[2] K. D. Ntouros, I. Z. Gitas, and G. N. Silleos, "Mapping agricultural crops with EO-1 Hyperion data," presented at the Hyperspectral Image and Signal Processsing: Evolution in Remote Sensing, 2009. WHISPERS '09. First Workshop on, Grenoble, France, 2009, pp. 1–4.

[3] J. Zabaiza *et al.*, "Novel Folded-PCA for improved feature extraction and data reduction with HSI and SAR in remote sensing," *ISPRS J. Photogramm. Remote Sens.*, vol. 93, pp. 112–122, 2014.

[4] M. K. Griffin, S. M. Hsu, H. Burke K., S. M. Orloff, C. A. Upham, and B. Misra, "Examples of EO-1 Hyperion Data Analysis," Lincoln Laboratory, MIT, Lexington, Massachusetts, HTAP-21, Jan. 2005.

[5] B. Xu and P. Gong, "Land-use/Land-cover Classification with Multispectral and Hyperspectral EO-1 Data," *Photogramm. Eng. Remote Sens.*, vol. 73, no. 8, pp. 955–965, Aug. 2007.

[6] J. Plaza, A. Plaza, R. Perez, and P. Martinez, "Parallel Classification of Hyperspectral Images using Neural Networks," in *Studies in Computational Intelligence*, vol. 133, Springer, pp. 193–216.

[7] S. Chen, X. Li, and L. Zhao, "Subpixel Mapping Method of Hyperspectral Images Based on Modified Binary Quantum Particle Swarm Optimization," *J. Electr. Comput. Eng.*, vol. 2017, pp. 1–17, 2017.

[8] G. P. Petropoulos, K. Arvanitis, and N. Sigrimis, "Hyperion hyperspectral imagery analysis combined with machine learning classifiers for land use/cover mapping," *Expert Syst. Appl.*, vol. 39, no. 3, pp. 3800–3809, Feb. 2012.

[9] C. Vaiphasa, "Consideration of smoothing techniques of hyperspectral remote sensing," *ISPRS J. Photogramm. Remote Sens.*, vol. 60, no. 2, pp. 91–99, 2006.

[10] "USGS EO-1." [Online]. Available: https://eo1.usgs.gov/. [Accessed: 11-Jan-2017].

[11] N. US Department of Commerce, "ESRL Global Monitoring Division - Global Radiation Group." [Online]. Available: https://www.esrl.noaa.gov/gmd/grad/solcalc/.

[12] J. Pearlman, S. Carman, C. Segal, P. Jarecke, P. Clancy, and W. Browne, "Overview of the Hyperion Imaging Spectrometer for the NASA EO-1 mission," 2001, vol. 7, pp. 3036–3038.

[13] G. Tharshini, G. Dinesh, G. M. R. I. Godaliyadda, and M. P. B. Ekanayake, "A Robust Expression Negation Algorithm for Accurate Face Recognition for Limited Training Data," presented at the 10th IEEE International Conference on Industrial and Information Systems, ICIIS - 2015, Colombo, Sri Lanka, 2015.

[14] T. Raiko, A. Ilin, and J. Karhunen, "Principal component analysis for large scale problems with lots of missing values," presented at the 18th European Conference on Machine Learning (ECML 2007), Warsaw, Poland, 2007.

[15] J. S. Tyo, A. Konsolakis, D. I. Diersen, and R. C. Olsen, "Principal-components-based display strategy for spectral imagery," *IEEE Trans. Geosci. Remote Sens.*, vol. 41, no. 3, pp. 708–718, Mar. 2003.

[16] M. Imani and H. Ghassemian, "Feature Space Discriminat Analysis for Hyperspectral Data Feature Reduction," *ISPRS J. Photogramm. Remote Sens.*, vol. 102, pp. 1–13, 2015.

[17] M. Sugiyama, "Dimensionality Reduction of Multimodal Labeled Data by Local Fisher Discriminant Analysis," *J. Mach. Learn. Res.*, vol. 8, pp. 1027–1061, Jan. 2017.

[18] M. Sugiyama, "Local Fisher Discriminant Analysis for Supervised Dimensionality Reduction," presented at the 23rd International Conference on Machine Learning, Pittsburgh, Pennsylvania, USA, 2006, pp. 905–912.

[19] W. S. K. Fernando, P. H. Perera, H. M. S. P. B. Herath, M. P. B. Ekanayake, G. M. R. I. Godaliyadda, and J. V. Wijayakulasooriya, "Video Event Classification and Anomaly Identification using Spectral Clustering," presented at the 15th International Conference on Advances in ICT for Emerging Regions (ICTer2015), Colombo, Sri Lanka, 2015.

[20] R. A. A. Rupasinghe, S. G. M. P. Senanayake, D. A. Padmasiri, M. P. B. Ekanayake, G. M. R. I. Godaliyadda, and J. V. Wijayakulasooriya, "Modes of Clustering for Motion Pattern Analysis in Video Surveillance," presented at the 8th IEEE International Conference on Information and Automation for Sustainability (ICIAfS - 2016), Galle, Sri Lanka, 2016.

[21] H. M. S. P. B. Herath, M. P. B. Ekanayake, G. M. R. I. Godaliyadda, and J. V. Wijayakulasooriya, "Multi-Feature based Hand Gesture Recognition," presented at the 15th International Conference on Advances in ICT for Emerging Regions (ICTer2015), Colombo, Sri Lanka, 2015.

[22] A. M. Fahim, A. M. Salem, A. Torkey, and M. A. Ramadan, "An Efficient enhanced k-means clustering algorithm," *J. Zhegiang Univ. - Sci. A*, vol. 7, no. 10, pp. 1626–1633, Oct. 2006.

[23] A. M. R. Abeysekara, T. S. J. Oorloff, S. S. P. Vithana, H. M. V. R. Herath, G. M. R. I. Godaliyadda, and M. P. B. Ekanayake, "Land Cover Classification and Sub Component Analysis Using Hyperspectral Imagery," in *IESL Transactions Part B*, Colombo, Sri Lanka, 2017, pp. 385–390.